BROADBAND RADIATION FROM PRIMARY ELECTRONS IN VERY ENERGETIC SUPERNOVAE

SHIN'ICHIRO ANDO

California Institute of Technology, Mail Code 130-33, Pasadena, CA 91125; ando@tapir.caltech.edu

AND

PETER MÉSZÁROS

Department of Astronomy and Astrophysics, Department of Physics, and Center for Particle Astrophysics, Pennsylvania State University,
University Park, PA 16802; nnp@astro.psu.edu

ABSTRACT

A class of very energetic supernovae (hypernovae) is associated with long gamma-ray bursts, in particular with a less energetic but more frequent population of gamma-ray bursts. Hypernovae also appear to be associated with mildly relativistic jets or outflows, even in the absence of gamma-ray bursts. Here we consider radiation from charged particles accelerated in such mildly relativistic outflows with kinetic energies of $\sim 10^{50}$ ergs. The radiation processes of the primarily accelerated electrons considered are synchrotron radiation and inverse Compton scattering of synchrotron photons (synchrotron self-Compton; SSC) and of supernova photons (external inverse Compton; EIC). In the soft X-ray regime, both the SSC and EIC flux can be the dominant component, but due to their very different spectral shapes, it should be easy to distinguish between them. When the fraction of the kinetic energy going into the electrons (ϵ_e) is large, the SSC is expected to be important; otherwise, the EIC will dominate. The EIC flux is quite high, almost independently of ϵ_e, providing a good target for X-ray telescopes such as *XMM-Newton* and *Chandra*. In the GeV gamma-ray regime, the EIC would be the dominant radiation process and the *Gamma-Ray Large Area Space Telescope* (*GLAST*, which has been renamed the *Fermi Gamma-ray Space Telesope*) should be able to probe the value of ϵ_e, the spectrum of the electrons, and their maximum acceleration energy. Accelerated protons also lead to photon radiation through the secondary electrons produced by the photopion and photopair processes. We find that over a significant range of parameters the proton component is generally less prominent than the primary electron component. We discuss the prospects for the detection of the X-ray and GeV signatures of the mildly relativistic outflow of hypernovae.

Subject headings: gamma rays: bursts — radiation mechanisms: nonthermal — supernovae: general

1. INTRODUCTION

While it is recognized that long gamma-ray bursts (GRBs) are associated with very energetic supernovae, sometimes referred to as hypernovae, our understanding of the physics that drives and connects these events is far from being established. Observationally, long GRBs are more complicated than were thought before. For example, they appear to have a subgroup that includes GRB 980425 (Galama et al. 1998), GRB 031203 (Malesani et al. 2004; Soderberg et al. 2004), and GRB 060218 (Campana et al. 2006; Cobb et al. 2006; Pian et al. 2006). These GRBs occurred relatively nearby and their energies radiated by prompt gamma rays were significantly smaller than the other long GRBs, and they were associated with well-studied hypernovae (SN 1998bw, SN 2003lw, and SN 2006aj, respectively). Radio observations of these events (Kulkarni et al. 1998; Soderberg et al. 2006) suggest the presence of mildly relativistic ejecta, which is a different component from the usual nonrelativistic component of the supernova explosion. Their rate of occurrence may be an order of magnitude higher than that of the more energetic GRBs (Liang et al. 2007; Soderberg et al. 2006). See also, e.g., Liang et al. (2006), Murase et al. (2006), Toma et al. (2007), Waxman et al. (2007), and Gupta & Zhang (2007) for other followup studies. Very recently, a mildly relativistic outflow component has also been inferred in a supernova of Type Ibc unassociated with a GRB, SN 2008D (Soderberg et al. 2008).

In this paper we investigate the broadband radiation from the mildly relativistic ejecta associated with hypernovae, focusing especially on the high-energy photon emission in the X-ray and gamma-ray ranges. We mainly study the radiation from relativistic electrons which are primarily accelerated in shocks, but we also consider the radiation from secondary electrons which are generated by interactions involving accelerated protons. The latter were extensively studied by Asano & Mészáros (2008) in connection with the origin of Galactic cosmic rays (Wang et al. 2007; Budnik et al. 2008). Our treatment of the proton component includes also the previously neglected effect of photopair production. We show that the primary electron component photon signature generally dominates over the proton component, for a wide range of energies. In particular, the inverse Compton scattering of hypernova photons due to the primary electrons appears the most promising channel for detection in the X-ray and gamma-ray ranges.

The paper is organized as follows. In § 2 we introduce the relevant supernova parameters and the spectrum of the primary accelerated electrons. We present our main results on the radiation from the primary electrons in § 3 and discuss its dependence on the parameters. Section 4 is devoted to a discussion of the photon radiation of proton origin and its comparison to the electron component. We summarize our conclusions in § 5.

2. SPECTRUM OF PRIMARY ELECTRONS

2.1. *Supernova Dynamics*

As suggested by Soderberg et al. (2006), there is an empirical relation between the kinetic energy (E_K) and the velocity (βc) of the hypernova ejecta, parameterized as $E_K = 10^{52}(\Gamma\beta/0.1)^{-2}$, where $\Gamma = (1 - \beta^2)^{-1/2}$. The low-velocity component with

$\Gamma\beta \simeq 0.1$ corresponds to a very energetic supernova, while the high-velocity component with $\Gamma\beta \simeq 1$ corresponds to the mildly relativistic ejecta. It is assumed that the energy of the ejecta components is dissipated when they start to decelerate, going into relativistic particles.

The deceleration occurs as a result of interaction with the surrounding matter, which we assume is provided by the mass loss of the massive progenitor (Wolf-Rayet type) star. We adopt a fiduciary mass-loss rate of $\dot{M} = 10^{-5}\ M_\odot$ and a wind velocity $v_w = 10^3$ km s^{-1}. The density profile is then $\rho(r) = (\dot{M}/4\pi v_w)r^{-2} = 5 \times 10^{11}r^{-2}$ g cm^{-1}. In this case, the kinetic energy ($E_K = 10^{50}$ ergs) of the mildly relativistic ejecta ($\Gamma\beta = 1$) starts to be dissipated when it reaches a radius $r = R \simeq 10^{16}$ cm. The corresponding dynamical timescale is $t_{\rm dyn} = R/c\Gamma\beta = 3 \times 10^5$ s, a few days. Around that time, the hypernova luminosity is still very large. On the other hand, if we consider subrelativistic but more energetic ejecta, the dynamical timescale is significantly larger, by which time the hypernova luminosity has decreased, a situation that is not interesting for the present purposes.

The hypernova luminosity around a few days after the explosion is roughly $L_{\rm SN} = 10^{43}$ ergs s^{-1}, and we assume the spectrum is blackbody with a temperature of ~ 1 eV; a typical photon energy is $\varepsilon_\gamma = 2.7$ eV. The photon number density at the dissipation radius R is then given by $n_\gamma = L_{\rm SN}/\pi c R^2 \varepsilon_\gamma = 4 \times 10^{11}$ cm^{-3}. We note that the parameter values above are very similar to those in Wang et al. (2007) and Asano & Mészáros (2008).

2.2. Acceleration and Cooling of Primary Electrons

When dissipation starts, we assume a fraction ϵ_e of the kinetic energy goes into primary electrons accelerated to relativistic speeds in the shock, and their initial spectrum is a power law with index $-p$. A typical Lorentz factor (in the ejecta frame) of the primary electrons is then given by $\gamma_m = \epsilon_e(m_p/m_e)\Gamma = 260(\epsilon_e/0.1)$. In addition, we assume a fraction ϵ_B of E_K goes into magnetic fields, yielding $B = [8\pi\epsilon_B\rho(R)c^2]^{1/2} = 1(\epsilon_B/10^{-2})^{1/2}$ G. We shall study the dependence of results on these parameters in the following, but unless otherwise stated, we adopt $\epsilon_e = 0.1$, $\epsilon_B = 10^{-2}$, and $p = 2.5$ as fiducial values, according to the analogy to GRB emission.

After acceleration, these electrons immediately lose their energies through radiation unless the cooling timescale $t_{\rm cool}$ is longer than the dynamical timescale $t_{\rm dyn}$. Relevant radiation mechanisms include synchrotron radiation due to magnetic field and inverse Compton scatterings off hypernova photons (external inverse Compton; EIC) and synchrotron photons (synchrotron self-Compton; SSC). The ratio of cooling timescales of EIC and synchrotron processes is given by $t_{\rm EIC}/t_{\rm syn} = U_B/\varepsilon_\gamma n_\gamma \approx 0.05(\epsilon_B/10^{-2})$. In addition, unless ϵ_e is much larger than ϵ_B, the SSC cooling timescale is at most comparable to that of synchrotron radiation. Thus, among those three, EIC is the most efficient mechanism for electron energy losses, and we have $t_{\rm cool} \approx t_{\rm EIC} < t_{\rm dyn}$ for $\gamma_e > \gamma_c \simeq 70$, where γ_e represents the electron Lorentz factor in the ejecta frame.

When the electrons are in the "fast-cooling" regime, defined as the case when $\gamma_c < \gamma_m$ (or equivalently $\epsilon_e > 0.03$ in the current context), the electron spectrum is given by

$$\frac{dN_e}{d\gamma_e} = \begin{cases} \dfrac{N_e}{\gamma_c}\left(\dfrac{\gamma_e}{\gamma_c}\right)^{-2}, & \gamma_c < \gamma_e < \gamma_m, \\[3mm] \dfrac{N_e}{\gamma_c}\left(\dfrac{\gamma_m}{\gamma_c}\right)^{-2}\left(\dfrac{\gamma_e}{\gamma_m}\right)^{-p-1}, & \gamma_e > \gamma_m, \end{cases} \quad (1)$$

where the normalization is set so that we have the correct number of electrons $N_e = E_K/\Gamma m_p c^2 = 5 \times 10^{52}$ after integration (e.g.,

Sari & Esin 2001). On the other hand, in the "slow-cooling" regime ($\gamma_c > \gamma_m$), we have

$$\frac{dN_e}{d\gamma_e} = \begin{cases} \dfrac{(p-1)N_e}{\gamma_m}\left(\dfrac{\gamma_e}{\gamma_m}\right)^{-p}, & \gamma_m < \gamma_e < \gamma_c, \\[3mm] \dfrac{(p-1)N_e}{\gamma_m}\left(\dfrac{\gamma_c}{\gamma_m}\right)^{-p}\left(\dfrac{\gamma_e}{\gamma_c}\right)^{-p-1}, & \gamma_e > \gamma_c. \end{cases} \quad (2)$$

3. RADIATION FROM PRIMARY ELECTRONS

3.1. Synchrotron Radiation

The synchrotron mechanism gives the dominant contribution at radio wave bands and also provides seed photons for the SSC process. The typical frequency and power from an electron with γ_e is

$$\nu_{\rm syn}(\gamma_e) = \frac{3eB}{4\pi m_e c}\gamma_e^2\Gamma, \quad (3)$$

$$P_{\rm syn}(\gamma_e) = \frac{c\sigma_{\rm T}}{6\pi}\gamma_e^2 B^2 \Gamma^2, \quad (4)$$

where $\sigma_{\rm T}$ is the Thomson cross section (Rybicki & Lightman 1979), and we define $\nu_m \equiv \nu_{\rm syn}(\gamma_m)$ and $\nu_c \equiv \nu_{\rm syn}(\gamma_c)$.

The flux of synchrotron photons $F_\nu^{\rm syn}$ is then given by

$$\frac{F_\nu^{\rm syn}}{F_{\nu,\rm max}^{\rm syn}} = \begin{cases} \left(\dfrac{\nu}{\nu_c}\right)^{1/3}, & \nu < \nu_c, \\[3mm] \left(\dfrac{\nu}{\nu_c}\right)^{-1/2}, & \nu_c < \nu < \nu_m, \\[3mm] \left(\dfrac{\nu_m}{\nu_c}\right)^{-1/2}\left(\dfrac{\nu}{\nu_m}\right)^{-p/2}, & \nu > \nu_m, \end{cases} \quad (5)$$

for the fast-cooling phase, and

$$\frac{F_\nu^{\rm syn}}{F_{\nu,\rm max}^{\rm syn}} = \begin{cases} \left(\dfrac{\nu}{\nu_m}\right)^{1/3}, & \nu < \nu_m, \\[3mm] \left(\dfrac{\nu}{\nu_m}\right)^{-(p-1)/2}, & \nu_m < \nu < \nu_c, \\[3mm] \left(\dfrac{\nu_c}{\nu_m}\right)^{-(p-1)/2}\left(\dfrac{\nu}{\nu_c}\right)^{-p/2}, & \nu > \nu_c, \end{cases} \quad (6)$$

for the slow-cooling phase, where $F_{\nu,\rm max}^{\rm syn} = N_e P_{\rm syn}(\gamma_e)/4\pi d^2 \nu_{\rm syn}(\gamma_e)$, and d is distance to the source (Sari et al. 1998). Here, we neglected the effect of synchrotron self-absorption, which however might become important at low-frequency radio bands.

We note that the radio flux at 10 GHz with this model and $d = 100$ Mpc is 1600 mJy for $\epsilon_e = 0.1$ and $\epsilon_B = 10^{-2}$ and 10 mJy for $\epsilon_e = 10^{-2}$ and $\epsilon_B = 10^{-4}$; the self-absorption is irrelevant at this frequency. For comparison, the radio fluxes around a similar frequency at a peak time were 0.5 mJy for GRB 060218 (Soderberg et al. 2006) and 50 mJy for GRB 980425 (Kulkarni et al. 1998). Given that the radio flux strongly depends on both ϵ_e and ϵ_B and that this model predicts a substantial flux, radio observations would enable a strong test to constrain these parameters or others.

If the magnetic fields are highly inhomogeneous on very small spatial scales, then the photon spectrum would be subject to another type of emission mechanism—jitter radiation (Medvedev

2000). In this case, the spectrum would be harder in the low-frequency range, $F_\nu \propto \nu$, below a jitter break frequency ν_{jm} (compare this with the $\nu^{1/3}$ dependence of the synchrotron radiation). Above ν_{jm}, on the other hand, the spectrum is the same as that of synchrotron. The break frequency ν_{jm} is typically larger than the synchrotron frequency $\min(\nu_c, \nu_m)$. The difference in these radiation mechanisms could be tested from observations. However, in the following, we assume that the magnetic fields are quasi-homogeneous, so the synchrotron radiation is preferred. This is because the shock waves we consider are close to the non-relativistic limit, where the generated magnetic fields would be more isotropic. Such a situation is far from that of ultrarelativistic GRBs where the jitter radiation has been mainly considered.

3.2. Inverse Compton Scattering

The SSC flux is straightforwardly obtained from the electron spectrum (eqs. [1] and [2]) and the synchrotron flux (eqs. [5] and [6]) through the expression

$$F_\nu^{\mathrm{SSC}} = \frac{3\sigma_{\mathrm{T}}}{4\pi R^2} \int d\gamma_e \frac{dN_e}{d\gamma_e} \int_0^1 dx\, g(x) F_{\nu_s}^{\mathrm{syn}}\left(\nu_s = \frac{\nu}{4\gamma_e^2 x}\right), \quad (7)$$

where $g(x) = 1 + x - 2x^2 + 2x \ln x$ (Rybicki & Lightman 1979; Sari & Esin 2001). What makes the argument here simpler compared with the usual GRB SSC model in the literature (e.g., Sari & Esin 2001; Zhang & Mészáros 2001; Gou & Mészáros 2007; Fan et al. 2008; Ando et al. 2008) is the fact that the electron cooling is overwhelmingly dominated by the interaction with the external supernova photons. This enables us to avoid solving the equations for $dN_e/d\gamma_e$ self-consistently.

The same expression can be used for EIC, with a slight modification, i.e., $F_\nu^{\mathrm{syn}} \to F_\nu^{\mathrm{SN}} = (L_{\mathrm{SN}}/4\pi d^2)\delta(\nu - \varepsilon_\gamma/h)$. Here, since the optical spectrum of a supernova can be approximated by a blackbody spectrum, which is relatively narrowband compared with, e.g., a synchrotron spectrum, we have assumed that it can be represented by a delta function in frequency. Then, the formula further simplifies to

$$F_\nu^{\mathrm{EIC}} = \frac{3\sigma_{\mathrm{T}}}{64\pi^2 R^2}\left(\frac{h\nu}{\varepsilon_\gamma}\right)^2 \frac{L_{\mathrm{SN}}}{\nu d^2} \int d\gamma_e\, \gamma_e^{-2} \frac{dN_e}{d\gamma_e} g\left(\frac{h\nu}{4\gamma_e^2 \varepsilon_\gamma}\right). \quad (8)$$

3.3. Results

In Figure 1 we show the photon flux νF_ν of the electron component as a function of photon energy, for a hypernova at a distance of $d = 100$ Mpc. The top and bottom panels correspond to the case of $\epsilon_e = 0.1$ (fast cooling) and 10^{-2} (slow cooling), respectively. We also plot the sensitivities of the *XMM-Newton* X-ray satellite (for a 100 ks exposure) and the *Gamma-Ray Large Area Space Telescope* (*GLAST*, which has been renamed the *Fermi Gamma-ray Space Telesope*, for a 3 day exposure); both exposure times are comparable to t_{dyn}. Note that we obtained the 3 day *GLAST* sensitivity from the published sensitivity of a one-year all-sky survey (equivalent to a 70 day exposure to each source)[1] by simply rescaling as $F_{\mathrm{sens}} \propto t^{-1/2}$. This is valid strictly only for the low-energy region where the sensitivity is limited by background. For the high-energy range, which is limited by photon counts, the sensitivity scales as $F_{\mathrm{sens}} \propto t^{-1}$ instead. However, understanding at which energy the transition happens requires a more careful study of the detector performance. For simplicity, we used the $t^{-1/2}$ dependence in the figure, because the detection would be dominated by low-energy photons around 100 MeV.
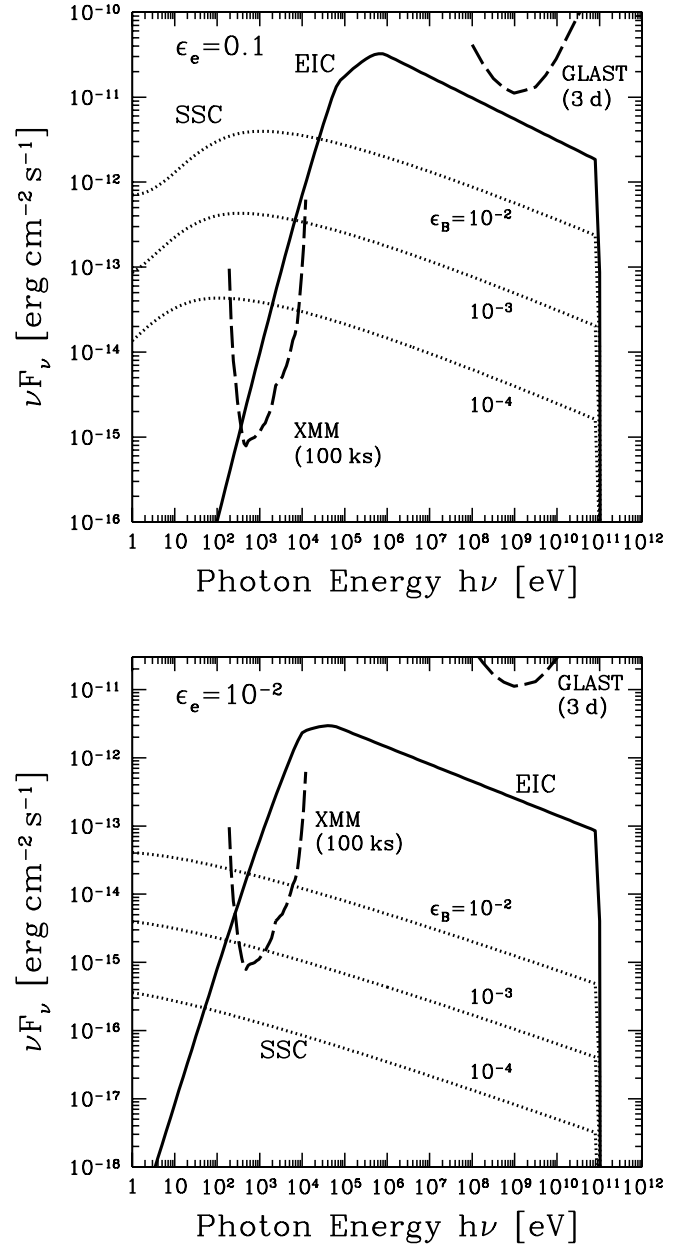
[1] See http://www-glast.slac.stanford.edu/.

FIG. 1.—Flux of EIC (*solid curves*) and SSC plus synchrotron (*dotted curves*) photons from a source at $d = 100$ Mpc, for $\epsilon_e = 0.1$ (*top*) and $\epsilon_e = 10^{-2}$ (*bottom*). Three dotted curves in each panel correspond to three different values of ϵ_B as labeled. The sensitivities of the *XMM-Newton* X-ray satellite as well as the *GLAST* gamma-ray satellite are shown as dashed curves. Note that the *GLAST* sensitivity for a 3 day exposure is obtained by a simple scaling as $t^{-1/2}$ (see text).

3.3.1. External Inverse Compton Scattering

The EIC flux has a very characteristic shape in the X-ray range, where its spectrum is quite hard. This is because the typical inverse Compton frequencies corresponding to γ_m and γ_c are above the X-ray region—i.e., $h\nu_m^{\mathrm{EIC}} \approx 4\Gamma\gamma_m^2\varepsilon_\gamma/3 = 350(\epsilon_e/0.1)^2$ keV and $h\nu_c^{\mathrm{EIC}} \approx 4\Gamma\gamma_c^2\varepsilon_\gamma/3 = 25$ keV—and in the X-ray range we see the low-energy tail of the external photons scattered by the least energetic electrons. This is consistent with the considerations of Waxman & Loeb (1999), who focused on emission from thermal electrons. In addition, as the electron distribution is determined by cooling by the EIC process with seed photons provided by an external source, the EIC flux is largely independent of ϵ_B, which is another useful feature enabling us to probe ϵ_e in a robust manner with X-ray measurements. In Figure 2 we show νF_ν^{EIC} at
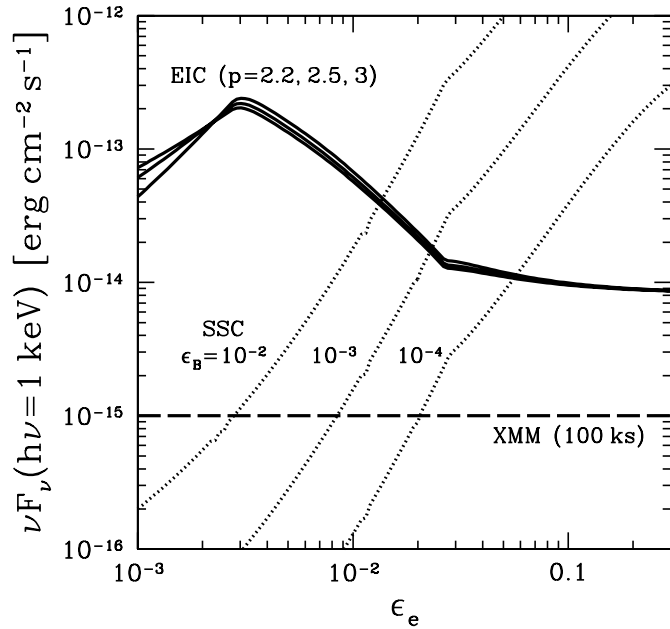
ANDO & MÉSZÁROS

FIG. 2.—Flux of EIC (*solid curves*) and SSC (*dotted curves*) photons at 1 keV as a function of ϵ_e for $d = 100$ Mpc. Three EIC (SSC) curves correspond to different values of p (ϵ_B), as labeled. The sensitivity of the current X-ray satellite is also shown as a horizontal line.

1 keV (*solid curves*) as a function of ϵ_e, for $d = 100$ Mpc. The shape of $\nu F_\nu^{\rm EIC}$ is roughly divided into the following three different regions.

1. The region $\epsilon_e < 3 \times 10^{-3}$ corresponds to electrons in the slow-cooling regime and $h\nu_m < 1$ keV $< h\nu_c$. Here, the typical Lorentz factor of the electrons that emit EIC photons at 1 keV ($\gamma_{\rm keV}$) satisfies $\gamma_m < \gamma_{\rm keV} < \gamma_c$, for which the electron distribution is given by the first expression of equation (2). From this expression, it is clear that increasing ϵ_e (or equivalently γ_m) makes the 1 keV flux larger, and the flux depends, albeit weakly, on the electron spectral index p.

2. The middle region $3 \times 10^{-3} < \epsilon_e < 0.03$ corresponds to 1 keV $< h\nu_m < h\nu_c$ (slow cooling). In this case, the flux is dominated by the tail emission from electrons with γ_m. Since the spectrum is hard at 1 keV ($\nu F_\nu \propto \nu^2$), it rapidly decreases as ν_m goes away from 1 keV (with increasing ϵ_e).

3. In the region with $\epsilon_e > 0.03$, the flux is almost independent of ϵ_e. The electrons are in the fast cooling regime, 1 keV $< h\nu_c < h\nu_m$. In this case, the flux at 1 keV is mostly due to tail emission of electrons with γ_c, whose numbers are little dependent on γ_m, as clearly seen in the first expression of equation (1).

In all cases, the soft X-ray flux is fairly high and robust and would be an excellent target for *XMM-Newton*.

In the GeV gamma-ray range, the EIC flux may be detected by *GLAST* if ϵ_e is large enough (Fig. 1). Although we have not assumed here any cutoff of the electron spectrum, the presence of such a cutoff as well as the spectral shape (characterized by p) could be tested with *GLAST*. The sharp cutoff seen around 10^2 GeV in Figure 1 is due to absorption by supernova photons, leading to electron-positron pairs (see discussion below). In Figure 3 we show the EIC flux integrated above 100 MeV (for $d = 100$ Mpc) plotted as a function of ϵ_e for three different values of p. Here, the *GLAST* sensitivity is rescaled using the $t^{-1/2}$ dependence and $t = t_{\rm dyn} \approx 3$ days, since the flux sensitivity above 100 MeV is in the background-limited regime (it becomes better if we use the *integrated* flux rather than the *differential* one
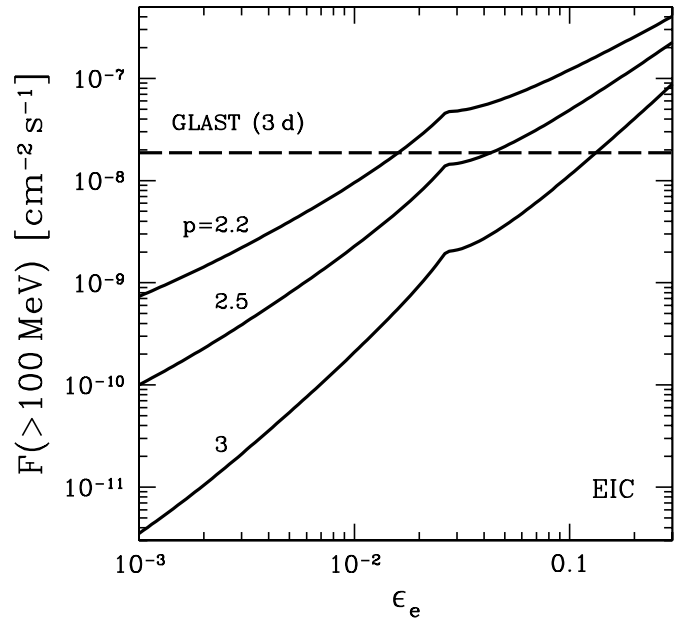

FIG. 3.—Flux of EIC photons integrated above 100 MeV as a function of ϵ_e for various values of p as labeled, for $d = 100$ Mpc. The *GLAST* sensitivity for a 3 day exposure is shown as a horizontal line.

shown in Fig. 1). For a hard electron spectrum, the EIC flux could be large in the GeV energy region for reasonable values of ϵ_e, so that *GLAST* should be able to probe the spectrum, including the maximum acceleration energy of the electrons.

3.3.2. *Synchrotron Self-Compton Scattering*

The SSC flux depends sensitively on both ϵ_e and ϵ_B, as shown in Figures 1 and 2. This would be a dominant component in the X-ray range, well within the sensitivity limit of X-ray telescopes, if both ϵ_e and ϵ_B are large enough. Since the spectral shape is very different from that of the EIC component, these components of two different origins should be easily distinguishable. In the GeV regime, on the other hand, the SSC flux is likely to be subdominant, unless ϵ_B is comparable to ϵ_e and as large as ~ 0.1.

As briefly argued at the end of § 3.1, if the generated magnetic fields were highly inhomogeneous on very small scales (although we believe this is unlikely in the current setup), then the synchrotron radiation would be replaced by another radiation component—jitter radiation (Medvedev 2000). The spectrum of the inverse Compton photons off the jitter radiation would be similar to the jitter spectrum, which results in a harder spectrum than SSC at low frequency. Therefore, the difference ($F_\nu \propto \nu$ vs. $\nu^{1/3}$) might appear in the X-ray regime and could be tested.

3.3.3. *Regenerated Emission due to Pair Production*

For photon energies $\gtrsim 10^2$ GeV, the $\gamma\gamma \rightarrow e^+e^-$ opacity against surrounding supernova photons becomes greater than unity (e.g., Stecker et al. 1992). Thus, these high-energy photons cannot escape from the source, giving a sharp cutoff in the spectrum as shown in Figure 1. The resulting $e^\pm$ pairs, having Lorentz factors above $\sim 10^5$, then radiate synchrotron photons over a wide frequency range. The inverse Compton scattering of supernova photons by these pairs occurs mainly in the Klein-Nishina regime, where the scattering cross section is suppressed (Rybicki & Lightman 1979), and can be neglected here.

The resulting pairs rapidly lose their energy through radiation, and thus, they are in the strongly fast-cooling regime. We computed the synchrotron spectrum from these pairs and show the
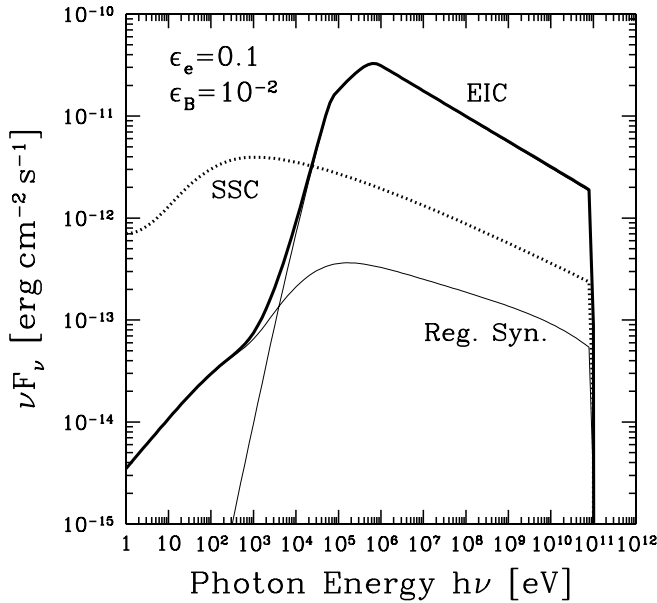
Fig. 4.—Synchrotron spectrum from electron-positron pairs ("regenerated" emission) produced by the interaction between high-energy EIC photons ($h\nu > 10^2$ GeV) and supernova photons (labeled as "Reg. Syn."). This flux is compared with other radiation components, SSC and EIC, for the fiducial parameter set and $d = 100$ Mpc.
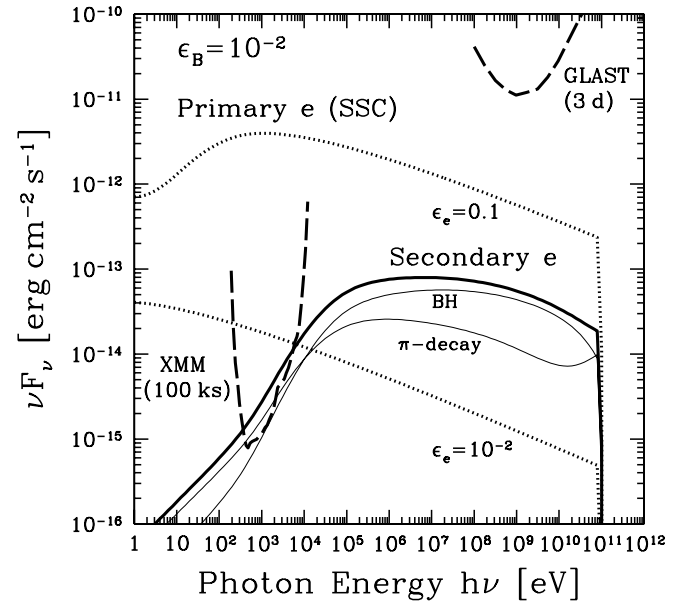
Fig. 5.—Flux of synchrotron photons from secondary electrons produced by proton interactions (*thick solid curve*), for $\epsilon_B = 10^{-2}$ and $d = 100$ Mpc. Components from π-decays and the Bethe-Heitler (BH) process are shown as thin solid curves. For comparison, the SSC spectrum from primary electrons for $\epsilon_e = 0.1$ and 10^{-2} are also shown as dotted curves.

results in Figure 4 for the fiducial case and $d = 100$ Mpc. We find that this radiation component is significantly lower than both the SSC and EIC components for all the available energy ranges. While we show here only the result for the fiducial case, the same conclusion would apply to other parameter sets, because the dependence of the regenerated emission on ϵ_e or ϵ_B is more or less the same as that of the SSC or EIC emission. In addition, if the EIC spectrum had any cutoff above 10^2 GeV, this would reduce even further the regenerated flux. Thus, the regeneration emission component can be safely ignored in the present discussion.

4. RADIATION FROM SECONDARY ELECTRONS AND PROTON ACCELERATION

Recently, Wang et al. (2007) and Budnik et al. (2008) suggested that hypernovae could account for some of the cosmic-ray flux that we measure today and also investigated the possibility of the associated neutrino emission and detection in order to further test such a scenario. Asano & Mészáros (2008) studied another consequence of this mechanism, the gamma-ray emission from secondary electrons produced by interactions involving accelerated protons. Their conclusion is that the synchrotron flux from these secondary electrons could be detected by modern X-ray telescopes. Here, we further extend their study, comparing the results with that of the primary electron component, and investigate which emission components would dominate in different energy ranges, depending on the parameters. As the origin of the secondary electrons, we consider decays of charged pions produced by interactions between protons and supernova photons, e.g., $p\gamma \rightarrow n\pi^+$ (labeled simply as $p\gamma$), and pair production through the Bethe-Heitler process, $p\gamma \rightarrow pe^+e^-$ (labeled as BH). The BH process was not taken into account in the computation of Asano & Mészáros (2008).

Following Wang et al. (2007) and Asano & Mészáros (2008), we assume that the total energy of cosmic-ray protons is $E_{cr} \simeq E_K/6$, and the energy distribution follows a ε_p^{-2} spectrum. The maxi-

mum acceleration energy of the protons is assumed to be given by $\varepsilon_{p,\max} = eBR\beta \simeq 2 \times 10^{18}(\epsilon_B/10^{-2})^{1/2}$ eV. We use again $\epsilon_B = 10^{-2}$ as our fiducial value, to compare with our primary electron radiation. Note that Asano & Mészáros (2008) used $\epsilon_B = 0.1$. Because of this our estimate results in slightly smaller fluxes than those of Asano & Mészáros (2008); as we argue below, the main dependence on ϵ_B is expected to be weak. The threshold energy for pion production through Δ-resonance is roughly given by $\varepsilon_{p,th}^{p\gamma} = 0.3$ GeV^2/$\varepsilon_\gamma \simeq 10^{17}$ eV; thus, protons with energies near $\varepsilon_{p,\max}$ can produce charged pions through this mechanism. The energy-loss timescale of the protons is given by $t_{p\gamma} = (0.2\sigma_{p\gamma}n_\gamma c)^{-1} \simeq 10^6$ s, where $\sigma_{p\gamma} = 5 \times 10^{-28}$ cm^2 (almost independent of energy) is the $p\gamma$ cross section and the factor 0.2 represents the energy lost by the proton by each interaction. The fraction of the total proton energy E_{cr} taken away by this process may then be estimated by $f_{p\gamma} = t_{dyn}/t_{p\gamma} \approx 0.2$. We assume that half of the outcomes of $p\gamma$ interactions are in the form of charged pions and that they carry off 20% of the parent proton energy, conserving the original ε_π^{-2} spectrum.

Secondary electrons or positrons are produced by pion decays, and we assume that their energies are 1/4 of that of the parent pions ($\varepsilon_e = 0.25\varepsilon_\pi = 0.05\varepsilon_p$), since a charged pion eventually decays into four light particles (one charged lepton and three neutrinos). The electron spectrum is again approximately represented by a power law with the same index, i.e., ε_e^{-2} for $6 \times 10^{15} < \varepsilon_e/\text{eV} < 10^{17}(\epsilon_B/10^{-2})^{1/2}$. These electrons rapidly lose their energy radiatively, and we obtain the final energy distribution by equating radiative energy loss and injection due to π production and decay. The typical energy of the synchrotron photons corresponding to $\varepsilon_e = 10^{16}$ eV is $\nu_{syn} \sim 10^{13}$ eV. Thus, the synchrotron spectrum from these secondary electrons is very hard and peaks in the multi-TeV region, where absorption by supernova photons is significant. A third generation of electrons and positrons is then produced, and they again radiate synchrotron photons, as discussed in § 3.3.3. We have included this process as well and show the spectrum due to this $p\gamma$ origin in Figure 5

(labeled as "π-decay"). The SSC spectra due to primary electrons are also shown for comparison, for the two cases of $\epsilon_e = 0.1$ and 10^{-2}. Although the flux itself from proton-originated leptons could be larger than the sensitivity of *XMM-Newton* for these parameters, a result consistent with that of Asano & Mészáros (2008), it is much less significant than the SSC component from primary electrons.

The Bethe-Heitler (BH) process can also be important for producing secondary electrons which radiate synchrotron photons in the relevant energy range. The BH cross section is $\sigma_{\mathrm{BH}} = (28/9)\alpha r_e^2 \ln(2\varepsilon_p\varepsilon_\gamma/m_p m_e c^4 - 106/9)$, where α is the fine-structure constant and $r_e = e^2/m_e c^2$ is the classical electron radius. The threshold energy of this interaction is then $\varepsilon_{p,\mathrm{th}}^{\mathrm{BH}} = (115/18)m_e m_p c^4/\varepsilon_\gamma \simeq 10^{15}$ eV, much smaller than the $p\gamma$ threshold $\varepsilon_{p,\mathrm{th}}^{p\gamma} \simeq 10^{17}$ eV. At each BH interaction, the proton loses energy by producing electron-positron pairs, and the magnitude is $\Delta\varepsilon_p = 2m_e c^2\gamma_{\mathrm{cm}}$, where $\gamma_{\mathrm{cm}} = (\varepsilon_p + \varepsilon_\gamma)/(m_p^2 c^4 + 2\varepsilon_p\varepsilon_\gamma)^{1/2} \approx \varepsilon_p/m_p c^2$ for the relevant ε_p range. Correspondingly, the energy of the produced electron or positron is $\varepsilon_e = m_e c^2\gamma_{\mathrm{cm}} \approx \varepsilon_p m_e/m_p = 5 \times 10^{-4}\varepsilon_p$. The energy-loss timescale of the proton is then given by $t_{\mathrm{BH}} = (\sigma_{\mathrm{BH}} n_\gamma c \Delta\varepsilon_p/\varepsilon_p)^{-1}$. The fraction of the total proton energy E_{cr} lost by this process is estimated as $f_{\mathrm{BH}} = t_{\mathrm{dyn}}/t_{\mathrm{BH}}$, which is typically ~ 0.01–0.03. We obtain the injection spectrum of these electrons and positrons by multiplying the proton spectrum by f_{BH}. Since f_{BH} is almost constant, this injection spectrum is again close to ε_e^{-2} for $5 \times 10^{11} < \varepsilon_e/\mathrm{eV} < 10^{15}(\epsilon_B/10^{-2})^{1/2}$; the final spectrum of the pairs is then obtained as the steady state solution of a diffusion equation including radiative energy losses. We find that the regenerated emission is negligible because the typical electron energy is much smaller than the $p\gamma$ case. We show the synchrotron spectrum from the BH process in Figure 5 and find that it is indeed comparable to the $p\gamma \rightarrow n\pi^+$ component. The lower fraction of total energy carried away ($f_{\mathrm{BH}} \ll f_{p\gamma}$) is compensated by the fact that pairs have lower energies, which radiate many photons in the relevant energy range such as soft X-rays.

Compared to the SSC photon component from the primary electron population, the photon component from a proton origin is significantly less important. This is also the case for other values of ϵ_B, because both components are related to synchrotron radiation, and the relative importance would not change much. Considering values of ϵ_e much smaller than 10^{-2} would change the proton-to-SSC ratio in favor of the former, but even in this case, the EIC component, which is not plotted explicitly in Figure 5, would still be very large in the soft X-ray regime as shown in Figure 2. This remains the case as long as $\epsilon_e \gtrsim 10^{-3}$. Using steeper spectra or smaller maximum acceleration energies for the protons simply reduces the proton yields; note that the $p\gamma$ process especially is very sensitive to these values. In the calculation above we used a very hard proton spectrum ε_p^{-2} and maximum efficiency for the acceleration, which is the best case for the proton component. Thus, the goal of testing proton acceleration in hypernovae and its connection to cosmic rays with X-ray or gamma-ray telescopes is hard to achieve, since the photon signatures would be largely swamped by a strong primary electron component. Neutrinos would remain the most reliable means of testing such a scenario.

Although difficult, we also mention two possibilities that might enable detection of a proton component in photon radiation. First, if one had situations such that $\epsilon_e \ll 10^{-3}$, where the bulk of the primary electrons might be nonrelativistic, whereas protons were accelerated efficiently in sufficiently large magnetic fields, then it might be possible to suppress the primary component compared with the secondary. Second, since the pro-

ton cooling times are longer than that of electrons, late-time observations might help the detection of a proton component, although adiabatic cooling and decaying flux levels would require long-time integrations.

5. CONCLUSIONS

We have studied the radiation from the mildly relativistic ejecta associated with hypernovae. The energy associated with this portion of the ejecta, about 10^{50} ergs, starts to dissipate at radii of about 10^{16} cm, where electrons and protons are shock accelerated. The electrons radiate photons via synchrotron, synchrotron self-Compton (SSC) of synchrotron photons, and external inverse Compton (EIC) scattering of hypernova photons. The radiation is most prominent in the X-ray and GeV ranges, detectable for sources at $d < 100$ Mpc. We also studied the radiation from the second and third generations of electrons and positrons that are associated with accelerated protons. The interactions that produce these leptons are the photopion and Bethe-Heitler (BH) processes, and both of these would give fluxes above the sensitivity limit of modern X-ray telescopes. However, we find that both of these components are hidden by a large flux due to the primary electron population mentioned above, for most realistic combinations of relevant parameters. Values of $\epsilon_e \ll 10^{-3}$ or very long lasting observations may improve the detection prospects of this component.

The most promising energy range for detecting the electron SSC and EIC emission components is in the soft X-ray range. If both ϵ_e and ϵ_B are reasonably large, the SSC component dominates, otherwise the EIC does (Fig. 2). The regenerated emission component from electron-positron pairs produced by $\gamma\gamma$ absorption of $\gtrsim 10^2$ GeV photons is found to be always negligible. A robust feature of the EIC emission is that it provides a fairly large flux in the X-ray regime, for most combinations of the parameters ϵ_e, ϵ_B, and p, if the supernova occurs at distances $d \leq 100$ Mpc. When the two components are comparable, it may be easy to distinguish them through their very different spectral shapes. The GeV flux is dominated by the EIC component. Observations with *GLAST* would make it possible to measure p independently, if ϵ_e is large enough, and would also be able to probe for the spectral cutoff corresponding to the maximum acceleration energy of the radiating electrons.

Finally, we briefly comment on the dependence of the results on the progenitor wind mass-loss rate. This is interesting in particular because Campana et al. (2006) estimated a substantial mass-loss rate $\dot{M} \sim 10^{-4}$ $M_\odot$ for the progenitor of GRB 060218/SN 2006aj, which is an order of magnitude larger than the nominal value adopted here. Such a higher mass loss rate decreases the dissipation radius R and the dynamical timescale t_{dyn} by an order of magnitude. Even if we decrease the supernova luminosity to $L_{\mathrm{SN}} = 10^{42}$ ergs s^{-1}, an order of magnitude below the nominal value adopted above, while keeping the other parameters the same, we find that both the SSC and EIC photon fluxes increase by about 2–3 orders of magnitude. This more than offsets the decrease by a factor 3 of the sensitivities of X-ray telescopes caused by the smaller t_{dyn}, implying a very significant further improvement in the prospects for detection.

REFERENCES

Ando, S., Nakar, E., & Sari, R. 2008, ApJ, in press (arXiv: 0807.0012)
Asano, K., & Mészáros, P. 2008, ApJ, 677, L31
Budnik, R., Katz, B., MacFadyen, A., & Waxman, E. 2008, ApJ, 673, 928
Campana, S., et al. 2006, Nature, 442, 1008
Cobb, B. E., Bailyn, C. D., van Dokkum, P. G., & Natarajan, P. 2006, ApJ, 645, L113
Fan, Y.-Z., Piran, T., Narayan, R., & Wei, D.-M. 2008, MNRAS, 384, 1483
Galama, T. J., et al. 1998, Nature, 395, 670
Gou, L.-J., & Mészáros, P. 2007, ApJ, 668, 392
Gupta, N., & Zhang, B. 2007, Astropart. Phys., 27, 386
Kulkarni, S. R., et al. 1998, Nature, 395, 663
Liang, E.-W., Zhang, B.-B., Stamatikos, M., Zhang, B., Norris, J., Gehrels, N., Zhang, J., & Dai, Z. G. 2006, ApJ, 653, L81
Liang, E.-W., et al. 2007, ApJ, 662, 1111
Malesani, D., et al. 2004, ApJ, 609, L5
Medvedev, M. V. 2000, ApJ, 540, 704
Murase, K., Ioka, K., Nagataki, S., & Nakamura, T. 2006, ApJ, 651, L5
Pian, E., et al. 2006, Nature, 442, 1011
Rybicki, G. B., & Lightman, A. P. 1979, Radiative Processes in Astrophysics (New York: Wiley-Interscience)
Sari, R., & Esin, A. A. 2001, ApJ, 548, 787
Sari, R., Piran, T., & Narayan, R. 1998, ApJ, 497, L17
Soderberg, A. M., et al. 2004, Nature, 430, 648
———. 2006, Nature, 442, 1014
———. 2008, Nature, 453, 469
Stecker, F. W., de Jager, O. C., & Salamon, M. H. 1992, ApJ, 390, L49
Toma, K., Ioka, K., Sakamoto, T., & Nakamura, T. 2007, ApJ, 659, 1420
Wang, X.-Y., Razzaque, S., Mészáros, P., & Dai, Z.-G. 2007, Phys. Rev. D, 76, 083009
Waxman, E., & Loeb, A. 1999, ApJ, 515, 721
Waxman, E., Mészáros, P., & Campana, S. 2007, ApJ, 667, 351
Zhang, B., & Mészáros, P. 2001, ApJ, 559, 110